Global Biogeochemical Cycles

RESEARCH ARTICLE
10.1029/2020GB006583

Recycling and Burial of Biogenic Silica in an Open Margin Oxygen Minimum Zone

A. W. Dale[1], K. M. Paul[2], D. Clemens[1], F. Scholz[1], U. Schroller-Lomnitz[1], K. Wallmann[1], S. Geilert[1], C. Hensen[1], A. Plass[1], V. Liebetrau[1], P. Grasse[3], and S. Sommer[1]

[1]GEOMAR Helmholtz Centre for Ocean Research Kiel, Kiel, Germany, [2]Ecosystems and Environment Research Programme, University of Helsinki, Helsinki, Finland, [3]German Centre for Integrative Biodiversity Research (iDiv) Halle-Jena-Leipzig, Leipzig, Germany

Key Points:

- Biogenic silica (BSi) preservation is high on the shelf and low under predominantly anoxic bottom waters
- BSi burial across the Peruvian margin down to 1,000 m water depth accounts for up to 7% of the global burial on continental margins
- Existing global data permit a simple relationship between BSi accumulation and rain rate

Supporting Information:

- Supporting Information S1

Correspondence to:
A. W. Dale,
adale@geomar.de

Citation:
Dale, A. W., Paul, K. M., Clemens, D., Scholz, F., Schroller-Lomnitz, U., Wallmann, K., et al. (2021). Recycling and burial of biogenic silica in an open margin oxygen minimum zone. *Global Biogeochemical Cycles*, *35*, e2020GB006583. https://doi.org/10.1029/2020GB006583

Received 19 FEB 2020
Accepted 16 DEC 2020

Author Contributions:
Conceptualization: A. W. Dale, K. M. Paul
Data curation: A. W. Dale, K. M. Paul, D. Clemens, F. Scholz, U. Schroller-Lomnitz, K. Wallmann, C. Hensen, A. Plass, V. Liebetrau, S. Sommer
Formal analysis: A. W. Dale, K. M. Paul, D. Clemens, F. Scholz, U. Schroller-Lomnitz, K. Wallmann, S. Geilert, C. Hensen, A. Plass, V. Liebetrau, P. Grasse, S. Sommer
Funding acquisition: A. W. Dale, K. Wallmann, C. Hensen, S. Sommer
Writing – original draft: A. W. Dale, K. M. Paul

Abstract An extensive data set of biogenic silica (BSi) fluxes is presented for the Peruvian oxygen minimum zone (OMZ) at 11°S and 12°S. Each transect extends from the shelf to the upper slope (~1,000 m) and dissects the permanently anoxic waters between ~200 and 500 m water depth. BSi burial (2,100 mmol m^{-2} yr^{-1}) and recycling fluxes (3,300 mmol m^{-2} yr^{-1}) were highest on the shelf with mean preservation efficiencies (34% ± 15%) that exceed the global mean of 10%–20%. BSi preservation was highest on the inner shelf (up to 56%), decreasing to 7% and 12% under anoxic waters and below the OMZ, respectively. The data suggest that the main control on BSi preservation is the rate at which reactive BSi is transported away from undersaturated surface sediments by burial and bioturbation to the underlying saturated sediment layers where BSi dissolution is thermodynamically and/or kinetically inhibited. BSi burial across the entire Peruvian margin between 3°S to 15°S and down to 1,000 m water depth is estimated to be 0.1–0.2 Tmol yr^{-1}; equivalent to 2%–7% of total burial on continental margins. Existing global data permit a simple relationship between BSi rain rate to the seafloor and the accumulation of unaltered BSi, giving the possibility to reconstruct rain rates and primary production from the sediment archive in addition to benthic Si turnover in global models.

1. Introduction

Silicic acid (H_4SiO_4) is an important nutrient for groups of phytoplankton such as diatoms and silicoflagellates (Dugdale et al., 1995). Silicic acid is biomineralized to amorphous biogenic silica (BSi, biogenic opal SiO_2) that constitutes the hard exoskeletons and tests of these organisms. Most BSi that is synthesized in the surface ocean is solubilized back to silicic acid in situ, with around one third of new production surviving dissolution in the ocean interior to reach the seafloor (Tréguer & De La Rocha, 2013). Around 80%–90% of the deposited flux is recycled back to silicic acid, such that only a minor fraction (<5%) of newly synthesized BSi is permanently buried in the sediment (Ragueneau et al., 2002; Tréguer & De La Rocha, 2013). Yet, the oceanic residence of silicic acid with regard to burial is short enough (~15 kyr), that the Si inventory will respond to changes in burial over glacial-interglacial timescales (Tréguer & De La Rocha, 2013; Tréguer et al., 1995). A sound understanding of BSi recycling efficiency is thus crucial for the biological carbon and silicon pumps (Dugdale et al., 1995; Tréguer et al., 2018), the assessment of paleoproductivity from the sedimentary BSi archive, and for more accurate global biogeochemical models (Gao et al., 2016; Heinze et al., 2003).

Upwelling areas in eastern boundary current systems are hotspots for silica biomineralization (Nelson et al., 1995). In the Peruvian upwelling region, primary production is most intense in austral summer and dominated by diatoms (Estrada & Blasco, 1985; Franz et al., 2012). It is sustained by nutrient-rich waters fed by the poleward-flowing Peru-Chile undercurrent (Echevin et al., 2008). Microbial respiration of sinking biogenic detritus leads to the formation of an oxygen minimum zone (OMZ) between ~100 and 500 m where dissolved oxygen is depleted down to levels that are functionally anoxic (Fuenzalida et al., 2009; Thamdrup et al., 2012). The sediments underlying the OMZ are classified as hemipelagic diatomaceous mud (DeMaster, 1981; Reimers & Suess, 1983). They accumulate massive amounts of particulate organic carbon (POC) at rates (per m^2) that are 5–6 times higher than the average continental margin value (Dale et al., 2015).

The burial efficiency of POC (i.e., burial/rain rate) is determined by the sediment accumulation rate and ambient oxygen concentrations (Canfield, 1993). Rapid burial of carbon away from the surface mixed layer reduces its exposure to oxidative attack, making permanent burial more likely (Hartnett et al., 1998). Mod-

Writing – review & editing: A. W. Dale, K. M. Paul, D. Clemens, F. Scholz, U. Schroller-Lomnitz, K. Wallmann, S. Geilert, C. Hensen, A. Plass, V. Liebetrau, P. Grasse, S. Sommer

erate sedimentation rates combined with a permanent lack of oxygen in the bottom water have thus been suggested to contribute to high POC burial efficiencies in the anoxic depths of the Peruvian OMZ (Dale et al., 2015; Reimers & Suess, 1983). The dependence of BSi preservation on oxygen levels is unknown. Most recent estimates suggest that around 0.5 ± 0.2 Tmol yr^{-1} of BSi (1 Tmol = 10^{12} moles) are permanently buried in upwelling sediments underlying oxygen-deficient waters (DeMaster, 2019). Current estimates of BSi burial on the margins (excluding deltas, estuaries, silica as sponge spicules, or authigenic clays) are 2.7–4.1 Tmol yr^{-1} (DeMaster, 2019; Ragueneau et al., 2010; Tréguer & De La Rocha, 2013). Given that sediments underling oxygen-deficient waters account for only a few percent of the total margin area (Helly & Levin, 2004), BSi burial may be elevated in these regions.

Despite the importance of coastal upwelling sediments for carbon sequestration, studies on BSi preservation have tended to focus on deep-sea settings (>1,000 m). BSi burial was formerly believed to have been dominated by the diatomaceous ooze belt surrounding Antarctica, accounting for two thirds of global burial (Tréguer et al., 1995). Concerns about lateral transport of sediment to the polar front motivated a data reassessment that led to a downscaling of the burial flux in the Southern Ocean by ~30% (from ca. 4.1–4.8 to 3.1 Tmol yr^{-1}) (DeMaster, 2002). It has been reduced further to 2.3 Tmol yr^{-1} (Chase et al., 2015). The corresponding global deficit was attributed to burial on the margins after scaling BSi burial to POC burial using a molar Si:C ratio of 0.6 or weight ratio of 3.1 (DeMaster, 2002). The shift in burial away from the Southern Ocean to the margins suggests a tighter coupling between the global sinks of Si and C than previously thought. More recently though, Rahman et al. (2017) argued that global Si burial as authigenic alumino-silicate minerals (clays) may be 4.5–4.9 Tmol yr^{-1}. However, the significance of authigenic Si to the global Si burial flux has been questioned (DeMaster, 2019).

The purpose of this paper is to determine rates of BSi recycling, burial and the preservation efficiency in sediments in, above and below the OMZ on the Peruvian margin and how they compare to the global data set. The discussion focusses on Si budgets and the putative controls on BSi preservation. The analysis is based on largely unpublished data from the Peruvian margin collected over five research campaigns along two transects extending from the shelf to the upper slope. The benthic Si data set presented here is, at the time of publication, the most comprehensive for a continental margin. This study advances previous investigations into benthic Si cycling on the Peruvian shelf (DeMaster, 1981; Froelich et al., 1988).

2. Material and Methods

2.1. Overview

Data are presented from nine stations along 11°S sampled during expedition M77 on RV Meteor (cruise legs 1 and 2) in November/December 2008 and 10 stations along 12°S during expedition M92 (leg 3) in January 2013 (Figure S1). Sampling stations on both transects ranged from ca. 80–1,000 m. Three of the stations at 11°S (St. 1.1, 4.1, and 4.2) are supplemental to the six stations discussed in a previous synthesis of POC burial (Dale et al., 2015). Nine of the stations along 12°S were revisited in April/May 2017 on expeditions M136 and M137 conducted consecutively. M77 and M92 took place during austral summer, that is, the low upwelling, high productivity season whereas M136 and M137 took place during the summer-winter transition. A wealth of benthic biogeochemical data has been published from these campaigns, focusing on the biogeochemistry of C, N, P, Fe, trace metals, and paleo aspects (e.g., Dale et al., 2019; Lomnitz et al., 2016; Scholz et al., 2011; Sommer et al., 2016). Here, we present a database of largely unpublished silicic acid fluxes (56 in total) and porewater distributions (63 sediment cores) from these sampling transects. Full details of sampling locations and data collected are listed in Tables S1 and S2. Silica data from three sites at 11°S (M77) have been previously reported by Ehlert et al. (2016). All Si data used in this study have been uploaded to the World Data Center PANGAEA (https://www.pangaea.de/).

In line with previous studies, the Peruvian margin is divided into three zones (Dale et al., 2015): (i) the middle and outer shelf (<ca. 200 m, O_2 generally below detection (dl, 5 μM) where nonsteady state conditions are occasionally driven by intrusion of oxygenated bottom waters (Gutiérrez et al., 2008), (ii) the core of the OMZ (ca. 200–~500 m (12°, Dale et al., 2015) or ~600 m (11°S, Bohlen et al., 2011) where O_2 is mostly < dl), and (iii) the deep oxygenated stations on the upper slope below the OMZ (O_2 > dl).

2.2. Benthic Silicic Acid Fluxes

Silicic acid fluxes were determined using time series data collected in situ using benthic incubation chambers (Biogeochemical Observatory landers [BIGO], Sommer et al., 2016). Lander fluxes were obtained by linearly interpolating the concentration-time series data. They provide the net recycling rate of BSi (BSi_{rec}):

$$BSi_{rec} = H\frac{d\left[H_4SiO_4\right]}{dt} \quad (1)$$

where $d[H_4SiO_4]/dt$ is the concentration-time gradient and H is the height of water in the chamber. The uncertainties associated with lander fluxes have been discussed in detail (Dale et al., 2015; Hammond et al., 2004; Tengberg et al., 2005). The mean standard error of each flux was equivalent to ±13% (range 2%–61%). For each station on each transect, we report the average of all fluxes determined at that station.

As an independent check on the chamber fluxes, the diffusive benthic silicic acid flux out of the sediment, J_{Diff}, was calculated from silicic acid pore water concentration gradients at the sediment surface using Fick's First Law (see supporting information). At each station, J_{Diff} ± SD was based on the average for all cores taken.

2.3. Sediment Sampling

Sediments were taken with a multiple-corer (MUC) and sub-sampled under anoxic conditions using an Ar-filled glove bag. Short 10 cm-diameter push-cores were also taken from the BIGO chambers immediately after they were returned to the deck and subsampled under Ar or air, depending on the cruise. The sectioning interval in the upper 5 cm was generally 0.5 cm (M92) or 1 cm (M77, M136, and M137), with increasing interval thickness moving down the core. Porewaters were extracted by centrifuge and filtered using cellulose acetate Nuclepore® filters (0.2 μm) inside the glove bag. Further sediment handling details are provided by Dale et al. (2016).

2.4. Analytical Details

Silicic acid concentrations were determined on board colorimetrically using standard photometric techniques (Grasshoff et al., 1999). Wet sediment samples were freeze–dried in the home laboratory for analysis of POC using a Carlo Erba elemental analyzer. POC content was determined in dry weight percent (%) after acidifying the sample with HCl (0.25 N) to release inorganic carbon (assumed to be carbonates) to CO_2. Total carbon (organic + inorganic) was determined using samples without acidification. Carbonate was determined by weight difference of the two measurements. The precision and detection limit of the POC analysis was 0.04% and 0.05%, respectively. The precision and detection limit of the carbonate analysis was 2% and 0.1%, respectively. Porosity was determined from the weight difference of the wet and freeze-dried sediment, assuming a sediment density of 2.5 g cm^{-3} and a seawater density of 1.023 g cm^{-3}.

The sediment cores where BSi measurements were performed are indicated in Tables S1 and S2. BSi was determined on 20 mg of freeze-dried ground sediment samples following the automatic NaOH leaching method of Müller and Schneider (1993). The precision of the method is 5%–10%. This operationally defined fraction has been shown to underestimate BSi content if diatom frustules are coated with authigenic metal oxides that protects them from dissolution (Michalopoulos & Aller, 2004; Rahman et al., 2017). Unless otherwise indicated, BSi from the Peruvian margin refers to unaltered opal and is reported as % SiO_2. Authigenic alumino-silicate minerals are also not extracted by the alkaline leach (Rahman et al., 2017), such that our BSi burial fluxes (and those in the wider literature) are minimum estimates of Si burial originally supplied to the sediment as unaltered opal.

The mass of terrigenous detrital (nonbiogenic) material was determined by mass difference of the total and biogenic components, that is, total mass – (carbonate + 2.8 × POC + BSi) where the factor 2.8 converts mass of POC to total particulate organic matter (Sayles et al., 2001). Terrigenous detritus in marine sediments

typically consists of alumino-silicates and (oxy)hydroxides weathered on land and transported to the ocean by rivers.

2.5. Excess ^{210}Pb and Sediment Accumulation Rates

Sediment accumulation (ω_{acc}, cm kyr^{-1}) was determined using measured unsupported activities of the particle-bound radionuclide ^{210}Pb (half-life 22.3 years) by gamma counting as described by Dale et al. (2015). The unsupported, or excess, ^{210}Pb ($^{210}Pb_{xs}$) is the fraction that is not produced by the decay of ^{222}Rn in the sediment but delivered to the seafloor with other particles. The mean error of the measurement was ~20%.

We used a steady-state reaction-transport model to calculate ω_{acc} by simulating the radioactive decay of $^{210}Pb_{xs}$ and transport by burial and mixing (bioturbation) (Alperin et al., 2002). Measured porosities at each station were used as input parameters along with the flux of $^{210}Pb_{xs}$ to the sediment surface. In taking this approach, we accept that sediment burial patterns on the continental margin are affected by resuspension and downslope redistribution of particulate material (Arthur et al., 1998; Erdem et al., 2016; Gutiérrez et al., 2009; Jahnke et al., 1990). Uncertainties in our ω_{acc} estimates due to discontinuities in radioisotope data by winnowing or mass wasting processes would require additional detailed sedimentological investigations (Salvatteci et al., 2014).

In a previous study (Dale et al., 2015), the adjustable model parameters (ω_{acc}, bioturbation coefficient and mixing depth) were constrained by visually fitting the model to $^{210}Pb_{xs}$ data. We have revaluated these parameters for both the 11°S and 12°S transects using a Monte Carlo-type approach that consisted of ensemble model simulations (10^3 runs) at each station using random sets of parameter values. The value of ω_{acc} was determined from the average of the 10 simulations with the minimum least squares regressions. The $^{210}Pb_{xs}$ data in some of the cores on the shelf were scattered in the upper 10 cm, leading to greater uncertainty in ω_{acc}, and in bioturbation coefficients that were not well constrained. We refer instead to the mixed layer thickness to compare bioturbation intensities between stations. In three cores at 12°S (128 and 195 m), the model was fit to the $^{210}Pb_{xs}$ below the apparent mixed depth. The data at 195 m were particularly scattered in cores sampled in 2008 (M92) and 2013 (M136), and the burial fluxes for this station should be treated cautiously. Additional analysis of shorter-lived tracers such as ^{7}Be (half-life 53 days) or photosynthetic pigments (e.g., chlorophyll a) would have been useful to make further inferences on sediment mixing intensity and whether slow mixing by animals below the apparent mixed may artificially increase our derived ω_{acc} values. ω_{acc} determined in cores from the same stations sampled in 2008 and 2013 at 12°S differed by 35% on average due to the downcore variability in ^{210}Pb and to local heterogeneity. We report the mean ω_{acc} for the stations sampled on two cruises at 12°S and all ω_{acc} are assigned a 35% uncertainty. For St. 2 and 4 at 11°S, no ^{210}Pb measurements were made and ω_{acc} for these sites was interpolated from adjacent stations. Parameters and boundary conditions for simulating $^{210}Pb_{xs}$ are given in Table S3.

2.6. Calculations and Definitions

The sediment accumulation rate was used to calculate the mass accumulation rate (MAR, g cm^{-2} yr^{-1}), that is, the total mass of biogenic + lithogenic material:

$$\mathrm{MAR} = \omega_{acc} \cdot \rho \cdot (1 - \varphi(L)) \quad (2)$$

where ρ is the dry density of solid particles and $\varphi(L)$ is the measured porosity of compacted sediment (see supporting information).

The accumulation rate of BSi (BSi_{acc}, g SiO_2 cm^{-2} yr^{-1}) was then calculated as:

$$BSi_{acc} = MAR \cdot \frac{BSi_{Av}(\%)}{100\%} \quad (3)$$

Conversion between mass and molar units was done using the molecular mass of SiO_2 (60.08 g mol^{-1}). In the above expression, BSi_{Av} (%) refers to the mean BSi content in sediment where dissolution of BSi no longer occurs, that is, below the depth of asymptotic silicic acid concentrations:

$$\mathrm{BSi}_{\mathrm{Av}} = \frac{1}{z-y}\int_{y}^{z}\mathrm{BSi}(x)\,\mathrm{d}x \tag{4}$$

where BSi(x) is the measured BSi content at depth x (cm), y is the depth where silicic acid concentrations reach their asymptotic value, and z is deepest BSi measurement depth. For the M92 data, $z = 10$ cm whereas during M77 the measurement depth varied, being up to 47 cm at St. 3. We made a simplifying assumption to calculate $\mathrm{BSi}_{\mathrm{Av}}$, whereby $\mathrm{BSi}_{\mathrm{Av}}$ was instead determined over the whole sediment core. We took this approach because the asymptotic depth is not that clear in all cores and fewer BSi data were available for 12°compared to 11°S (see supporting information). The reported uncertainty in $\mathrm{BSi}_{\mathrm{Av}}$ is the standard deviation of all BSi(x) at each station. The uncertainty in $\mathrm{BSi}_{\mathrm{acc}}$ was determined from MAR and $\mathrm{BSi}_{\mathrm{Av}}$ using standard error propagation rules.

The rain rate of BSi to the seafloor was assumed equal to the sum of $\mathrm{BSi}_{\mathrm{acc}}$ and the fraction of BSi that is recycled to silicic acid (determined using the BIGO landers):

$$\mathrm{BSi}_{\mathrm{RR}} = \mathrm{BSi}_{\mathrm{acc}} + \mathrm{BSi}_{\mathrm{rec}} \tag{5}$$

For stations 1.1, 4.1, and 4.2 at 11°S where no benthic chambers were deployed, $\mathrm{BSi}_{\mathrm{rec}}$ was estimated from a linear relationship between J_{Diff} and $\mathrm{BSi}_{\mathrm{rec}}$ determined from the other sites (see Section 3.2).

Finally, the burial efficiency of BSi (BSiBE, %) was calculated as:

$$\mathrm{BSiBE} = \frac{\mathrm{BSi}_{\mathrm{acc}}}{\mathrm{BSi}_{\mathrm{RR}}}\cdot 100\% \tag{6}$$

The uncertainty in BSiBE was calculated using standard error propagation rules. The major assumptions implicit in Equation 6 are as follows: (i) the fluxes are in steady state, and (ii) that dissolution of BSi is the only reaction affecting silicic acid and BSi within the sediment pile.

Mean $\mathrm{BSi}_{\mathrm{RR}}$ and $\mathrm{BSi}_{\mathrm{acc}}$ per transect and for both transects combined were calculated by weighting the data from each station according to the distance between adjacent stations. Mean values of BSiBE were determined in the same way, instead of using Equation 6 with the mean $\mathrm{BSi}_{\mathrm{acc}}$ and $\mathrm{BSi}_{\mathrm{RR}}$. The distance-weighted arithmetic mean provides a more realistic estimate of the overall BSiBE because it considers the individual characteristics of the Si budget at each site.

Organic carbon burial efficiencies (CBE) at 12°S were calculated analogously using POC accumulation rates and benthic dissolved inorganic carbon (DIC) fluxes (Dale et al., 2015). The CBEs reported here for the 12°S transect have been revised from those given in Dale et al. (2015) to account for the new data on POC content, ω_{acc}, and DIC fluxes from the most recent expeditions (M136 and M137). The CBEs for 11°S have also been revised with the new ω_{acc} estimates from the ensemble model runs. The CBEs are more uncertain for 11°S than at 12°S since the recycling flux was estimated using modeled data rather than measured DIC fluxes (Bohlen et al., 2011). The mean relative difference in CBE estimates at each station from the values reported by Dale et al. (2015) was 17%.

2.7. Existing Literature Data for BSiBE, $\mathrm{BSi}_{\mathrm{RR}}$, and $\mathrm{BSi}_{\mathrm{acc}}$

Published literature data (Table 1) for BSiBE, $\mathrm{BSi}_{\mathrm{RR}}$, and $\mathrm{BSi}_{\mathrm{acc}}$ are available from four regions in the Southern Ocean and nine other deep-water regions (>1,000 m). The shallower sites are oxygen-deficient margins in Guaymas Basin (O_2, < dl), San Pedro Basin, and San Nicolas Basin on the California Borderlands (low and variable O_2, < ~20 μM, Berelson, 1991) plus additional data from the Peruvian shelf by Froelich et al. (1988). BSi rain rates in the studies listed in Table 1 were mainly calculated as the sum of the recycling and burial fluxes assuming steady state. Recycling fluxes were estimated from porewater profiles or benthic chamber data. Burial fluxes were generally estimated using MAR and BSi contents determined by alkaline leaching, but not always using the same geochronology. The data listed are the mean values for each specific region, taken directly from a data compilation by Ragueneau et al. (2009) (Indian Ocean, NW Atlantic, NE Atlantic, Equatorial Atlantic) or calculated by ourselves as the arithmetic mean of the individual sampling

Table 1
Published Si Data Used in This Study[a]

Region	Water depth (m)	Sediment accumulation (cm kyr^{-1})	BSi content (%)	BSi accumulation (mmol Si m^{-2} yr^{-1})	BSi recycling (mmol Si m^{-2} yr^{-1})	BSi rain rate (mmol Si m^{-2} yr^{-1})	BSi burial efficiency (%)
			Southern Ocean				
170°W transect "/>	2,740–4,967	2.7 (0.5–8.2)	62 (27–92)	84 (9–273)	649 (126–1,215)	734 (135–1,403)	10 (5–19)
Ross Sea[c]	572–3,580	4.1 (1.1–16)	9 (1–43)	189 (3–1,233)	356 (108–890)	545 (114–2,124)	13 (1–58)
POOZ[d]	3,620–4,710	6.7	~79	280	1,675	1,955	14
PFZ[d]	4,240–4,600	2.4	41–69	88	733	821	11
			Other regions				
Eq. Pacific[e]	3,150–4,620	0.9 (0.1–1.7)	14 (11–16)	7 (1–19)	98 (56–159)	105 (57–178)	5 (2–11)
Eq. Pacific[f]	4,391–4,560	1.7 (0.9–2.7)	5 (2–8)	10 (2–16)	133 (84–172)	144 (86–180)	7 (3–10)
N. Pacific[g]	4,783–5,741	0.7 (0.2–1.5)	3 (1–8)	2 (0.1–8)	87 (15–243)	89 (15–245)	2 (1–5)
N. Pacific[h]	4,427–5,679	0.6 (0.2–1.0)	15 (7–28)	4 (1–9)	253 (77–389)	257 (80–390)	1.9(0.3–3)
NE Pacific[e]	2,200–4,230	7.8 (1.3–19)	6 (3–10)	42 (4–141)	236 (51–653)	278 (55–794)	12 (7–18)
NW Indian Ocean[i]	4,059	4.0	6	18	260	278	6
NW Atlantic (BATS)[i]	~4,300	0.7	<2	1	17	18	6
NE Atlantic (PAP)[i]	~4,800	7.5	1–2	8	57	65	12
Eq. Atlantic C[j]	~4,000	100	4–6	172	274	446	39
Eq. Atlantic D[j]	~4,000	120	3–5	307	614	921	33
Guaymas Basin[k]	665	180	16	941	743	1,683	56
Peru Shelf[l]	86–183	297 (230–360)	10 (8–12)	591 (358–827)	1,961 (1,023–2,997)	2,552 (1,380–3,585)	24(16–31)
California Borderland[m]	900–1,800	70 (38–101)	~0.3	25	256	280	8.7

[a]Where reported, mean values are given with the range of observed values in parentheses. POOZ, Permanently Open Ocean Zone, PFZ, Polar Front Zone, BATS, Bermuda Atlantic Time-series Study, PAP, Porcupine Abyssal Plain. [b]Sayles et al. (2001), 7 stations across siliceous ooze in the Pacific Basin. Burial flux based on ^{230}Th-normalized sediment accumulation rates in upper 5 cm; recycling flux based on porewater dissolved silicic acid gradients; rain rate for the individual stations was calculated as the recycling plus burial flux. BSi content based on the formula SiO_2-($0.4H_2O$). [c]DeMaster et al (1996). Recycling flux based on ex situ whole core incubations; burial flux based on ^{14}C chronology; rain rate calculated as recycling plus burial fluxes. Only stations where the recycling flux was measured were considered in the calculations (St. 90-1, 90-30, 90-40, 90-110, 92-55, 92-137, 92-141). We excluded the rapidly accumulating sediments in Granite Harbor. [d]Recycling fluxes for the POOZ and the PFZ are model results by Rabouille et al. (1997), taking here the average of cores KTB06 and KTB05 for the POOZ, and cores KTB11, KTB13, KTB16 for the PFZ (their Table 4). BSi content from these cores were taken from Figure 9 in Rabouille et al. (1997) after converting their values in wt.% Si to % SiO_2 by multiplying by 60/28. BSi accumulation rates are the average of the ^{230}Th-normalized data given by Pondaven et al. (2000) and Francois et al. (1997) for the Indian Sector of the Southern Ocean reported by DeMaster (2002). Rain rate calculated in this study as recycling plus burial fluxes. The ^{230}Th-normalized BSi burial flux for the POOZ and PFZ is ~70% and 25%, respectively, of the values reported by Rabouille et al. (1997), who assumed a sedimentation rate of 10 cm kyr^{-1}. Correcting Rabouille et al.'s sedimentation rate by the same proportions as the BSi burial fluxes leads to a rough estimate of the sedimentation rates for the POOZ and PFZ of 6.7 and 2.4 cm kyr^{-1}, respectively. These values are provided to complete the table but not used in the calculations. [e]Dymond and Lyle (1994), Stations H, M, S, C in the equatorial Pacific and MZF, JDF, NS, MW, and G in the NE Pacific. Burial flux based on ^{230}Th, ^{14}C and oxygen isotopic stratigraphy; rain rate based on long-term (~≥1 year) sediment trap deployments corrected for resuspension; recycling flux calculated as the difference between rain rate and burial fluxes. BSi contents are reported in Archer et al. (1993). [f]McManus et al. (1995) and Berelson et al. (1997). Seven stations from 5°N to 5°. Burial flux based on ^{14}C accumulation rates. Recycling flux based on benthic chamber fluxes and porewater gradients. Rain rate calculated in this study as recycling plus burial fluxes. [g]Hou et al. (2019). Five roughly meridional stations (148°W-157°W) in the NW Pacific. Burial flux based on previously published paleomagnetic averages over the last 700 kyr. Recycling flux based on porewater gradients. Rain rate calculated as recycling plus burial fluxes. [h]Shibamoto and Harada (2010). Four stations in the western N. Pacific. Burial flux based on ^{230}Th/^{232}Th activity ratios. Recycling flux based on porewater gradients. Rain rate calculated as recycling plus burial fluxes. [i]From the data compiled by Ragueneau et al. (2009) in their Table 3. Rain rates calculated as recycling plus burial fluxes. Water depths and BSi contents from references therein. [j]Ragueneau et al. (2009), BIOZAIRE stations C and D in the Congo submarine canyon. Burial flux based on excess ^{210}Pb measurements; Recycling flux based on porewater gradients. Rain rate calculated as recycling plus burial fluxes. [k]Recycling flux and BSi accumulation calculated from data in Geilert et al. (2020) for a site (27°42.41′ N and 111°13.66′ W) on the slope underlying bottom waters with O_2 concentrations below analytical detection limit of the Winkler titration. Rain rate calculated in this study as recycling plus burial fluxes. [l]Froelich et al. (1988) report sedimentation rates, BSi and silicic acid data for six stations on the Peruvian margin. Data included in this study were taken from shelf stations BX-4, BX-5, and BX-6. Stations BX-2, BX-3, and GS-6 were not included because of nonsteady state artifacts (BX-3 and GS-6) or a large sampling depth interval at the surface sediment where BSi_{rec} cannot be accurately calculated (BX-2). Rain rate calculated in this study as recycling plus burial fluxes. [m]Berelson et al. (1987). Average for San Pedro and San Nicolas Basins (their Table 8). Recycling flux based on benthic chamber fluxes. The sediment accumulation rate was calculated from the MAR given in Berelson et al. (1987) assuming a density of 2.2 g cm^3 and a porosity of 0.82 (Leslie et al., 1990). These values are provided to complete the table but not used in the calculations.

Table 2
Mass Accumulation Rates and Sediment Silicon Budget at 11°S and 12°S on the Peruvian Margin

Station	Water depth (m)	Sediment accumulation rate (ω_{acc}) (cm kyr^{-1})	Mass accumulation rate (MAR) (g m^{-2} yr^{-1})	Mean BSi content (BSi_{Av}) (%)	BSi accumulation (BSi_{Acc}) (mmol m^{-2} yr^{-1})	BSi recycling (BSi_{Rec}) (mmol m^{-2} yr^{-1})	BSi rain rate (BSi_{RR}) (mmol m^{-2} yr^{-1})	BSi burial efficiency (BSiBE) (%)	POC burial efficiency (CBE)[a] (%)
					11°S				
1	82	350 ± 120	1,400 ± 490	12 ± 2.9	2,800 ± 1,200	3,200 ± 210	5,900 ± 1,200	47 ± 22	52 ± 24
1.1	145	44 ± 15	110 ± 40	17 ± 3.7	320 ± 130	4,000 ± 1,000	4,400 ± 1,000	7.4 ± 3.5	No data
2	259	53 ± 19	120 ± 41	11 ± 3.0	220 ± 96	4,600 ± 580	4,900 ± 580	4.5 ± 2.0	34 ± 13
3	311	62 ± 22	190 ± 65	6.6 ± 2.7	200 ± 110	2,400 ± 420	2,600 ± 440	7.8 ± 4.4	49 ± 20
4	397	38 ± 13	270 ± 96	4.0 ± 2.5	180 ± 130	2,500 ± 200	2,700 ± 240	6.7 ± 4.9	51 ± 29
4.1	512	14 ± 4.9	67 ± 24	1.0 ± 0.3	12 ± 5.0	1,000 ± 250	1,000 ± 250	1.1 ± 0.6	No data
4.2	579	34 ± 12	200 ± 71	0.6 ± 0.6	21 ± 21	840 ± 210	860 ± 210	2.5 ± 2.5	No data
5	695	73 ± 26	420 ± 150	1.4 ± 0.7	100 ± 58	700 ± 120	810 ± 130	13 ± 7.5	77 ± 36
6	978	57 ± 20	390 ± 140	1.4 ± 0.6	90 ± 51	1,500 ± 460	1,600 ± 460	5.5 ± 3.5	63 ± 27
					12°S				
1	74	470 ± 170	1,900 ± 660	14 ± 2.1	4,500 ± 1,700	3,500 ± 360	7,900 ± 1,700	56 ± 25	19 ± 9
2	101	320 ± 110	630 ± 220	19 ± 2.4	2,000 ± 740	4,000 ± 420	5,900 ± 850	34 ± 13	17 ± 6
3	128	140 ± 50	340 ± 120	22 ± 4.4	1,200 ± 502	2,800 ± 180	4,200 ± 530	29 ± 13	24 ± 9
4	142	72 ± 25	230 ± 80	15 ± 2.4	580 ± 220	2,000 ± 140	2,500 ± 260	23 ± 9.1	37 ± 14
5	195	140 ± 49	450 ± 160	13 ± 0.5	990 ± 350	2,700 ± 150	3,600 ± 380	27 ± 9.9	61 ± 26
6	244	47 ± 16	120 ± 43	8.8 ± 0.9	180 ± 66	1,300 ± 180	1,500 ± 190	12 ± 4.6	39 ± 16
7	306	50 ± 17	150 ± 52	7.9 ± 0.3	200 ± 69	670 ± 79	870 ± 110	23 ± 8.5	66 ± 29
8	409	9.0 ± 3.2	36 ± 13	2.5 ± 2.4	15 ± 15	390 ± 36	400 ± 40	3.8 ± 3.8	23 ± 10
9	756	47 ± 16	340 ± 120	1.0 ± 0.3	59 ± 26	530 ± 78	590 ± 82	10 ± 4.5	56 ± 26
10	989	60 ± 21	540 ± 190	1.3 ± 0.2	110 ± 42	470 ± 140	580 ± 140	19 ± 8.6	70 ± 33
					Averages 11°S and 12°S				
Shelf		250 ± 87	910 ± 320	15 ± 2.7	2,100 ± 830	3,300 ± 400	5,300 ± 1,000	34 ± 15	30 ± 13
OMZ		37 ± 13	150 ± 51	5.2 ± 1.8	130 ± 66	1,900 ± 260	2,000 ± 270	6.7 ± 3.8	32 ± 14
Below OMZ		59 ± 21	430 ± 150	1.3 ± 0.4	90 ± 43	790 ± 190	880 ± 200	12 ± 6.1	66 ± 30
All		110 ± 39	460 ± 160	7.7 ± 1.7	760 ± 310	2,100 ± 290	2,800 ± 500	17 ± 8.2	39 ± 18

Note. The shaded rows distinguish the OMZ stations from the shelf and deeper sites. Fluxes are moles of Si. Data are rounded to two significant figures[b].
[a]CBE values updated from Dale et al. (2015). [b]Uncertainty calculation (±) are explained in Section 2.

sites (Southern Ocean 170°W transect, Ross Sea, North Pacific, and Equatorial Pacific. Mean BSiBE varied between ~6% (Bermuda Atlantic Time-series Study site) and 56% (Guaymas Basin).

3. Results

3.1. Mixing Depths and Sediment Accumulation Rates

$^{210}Pb_{xs}$ at most stations decreased in a quasiexponential manner (Figures S2–S4). Three shelf stations (St. 1 at 11°S, St. 3 and 5 at 12°S during 2013, and St. 5 during 2017) exhibited considerable scatter, presumably due to intermittent bioturbation during periods of bottom water ventilation (Gutiérrez et al., 2008). The mixed layer thickness determined by ensemble modeling of $^{210}Pb_{xs}$ decreased substantially from the shelf (0.2–13.4 cm, median 7.6 cm) to the OMZ and below (0.1–4.2 cm, median 0.4 cm) (Table S3). Sediment accumulation rates ranged from 9 cm kyr^{-1} in the OMZ at St. 8 (12°S) to 470 cm kyr^{-1} on the shelf at St. 1 (12°S) (Table 2).

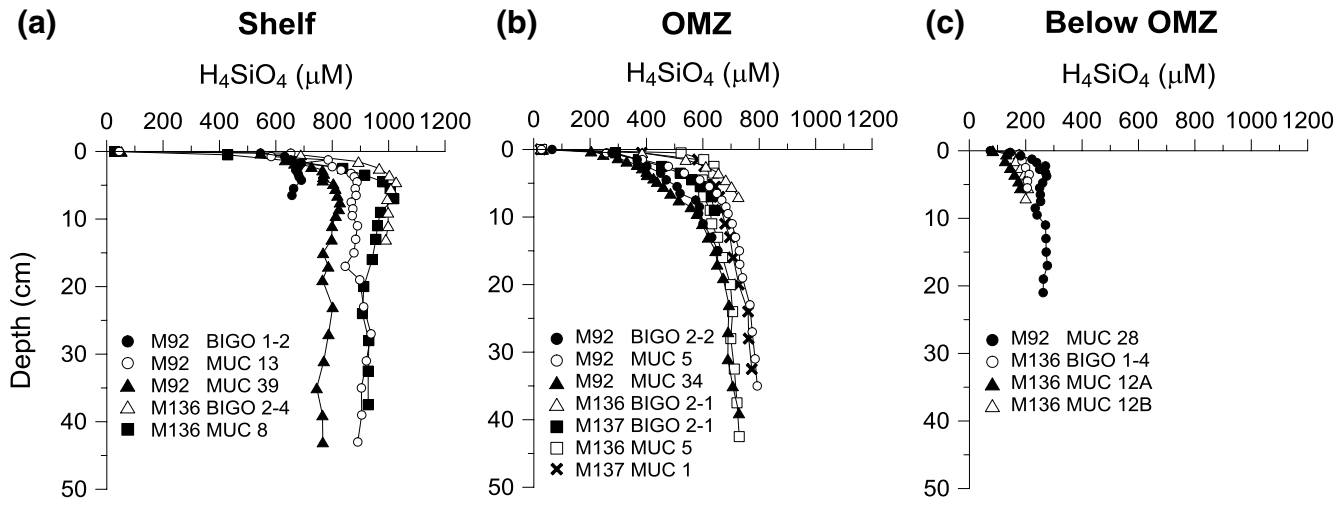

Figure 1. Silicic acid concentrations in sediment porewaters on the shelf (St. 1, 74 m), OMZ (St. 6, 244 m), and below the OMZ (St. 10, 989 m) at 12°S. Profiles from all cores are shown in Figures S5 and S6.

The lowest MAR were found for the OMZ at St. 4.1 (11°S) and St. 8 (12°S) where sediment deposition is inhibited by winnowing (Table 2). Highest MAR of 1,900 g m^{-2} yr^{-1} were found on the shelf; a factor of 3–4 higher than the global shelf average of 500 g m^{-2} yr^{-1} (Burwicz et al., 2011). On average, the MAR for stations below the OMZ were twice as high as for stations within the OMZ (150 vs. 430 g m^{-2} yr^{-1}), likely due to down slope transport and deposition of particles resuspended from the shelf (Arthur et al., 1998; Dale et al., 2015).

It is important to note that the ω_{acc} and MAR values are characteristic of the lifetime of ^{210}Pb (i.e., ~100 years). Long-term accumulation rates determined from ^{14}C data indicate episodic removal of sediments through mass-wasting or scouring (DeMaster, 1981). The computed ω_{acc} values are thus upper limits to the long-term (millennial) rates that should be used construct global silica budgets.

3.2. Silicic Acid in Porewaters

Examples of porewater silicic acid concentrations for the shelf, OMZ, and below the OMZ are shown in Figure 1 for 12°S (all cores are shown in Figures S5 and S6). Concentrations increased from bottom water values of 30–80 μM to quasiasymptotic values at depth below the sediment-water interface ($H_4SiO_{4\infty}$). $H_4SiO_{4\infty}$ generally decreased with water depth from 700 to 900 μM on the shelf to ~200 μM below the OMZ (Figure S7). Given that bottom water temperature decreased from ca. 15° to 5°C across the margin (Figure S11), the decrease in $H_4SiO_{4\infty}$ is consistent with thermodynamic (solubility) control on silica dissolution (Van Cappellen & Qiu, 1997a, 1997b). Yet, at all stations, $H_4SiO_{4\infty}$ was well below the theoretical solubility of opal ($H_4SiO_{4\_SAT}$) that decreased from 1,164 to 953 μM across the transect (Figure S7). Qualitatively similar trends have been observed around the world (Hurd, 1973). This points toward further controls on $H_4SiO_{4\infty}$ such as detrital content and sediment accumulation rates, as discussed later.

Diffusive silicic acid fluxes decreased from ~4,000 mmol m^{-2} yr^{-1} on the shelf to ~300 mmol m^{-2} yr^{-1} below the OMZ (not shown). At 12°S, these fluxes were very similar to BSi_{rec} determined using the benthic chambers, whereas at 11°S BSi_{rec} was 60% higher (Figure S8). For stations 1.1, 4.1, and 4.2 at 11°S where no in situ fluxes were available, BSi_{rec} was thus determined as $J_{Diff} \times 1.6$. A higher flux in benthic chambers is often attributed to enhanced pumping of porewater by tube-dwelling organisms (Glud et al., 1994). Given the lack of large communities of burrowing organisms in the OMZ, a better agreement between the two approaches might have been expected at 11°S. At present there is no clear explanation for these differences.

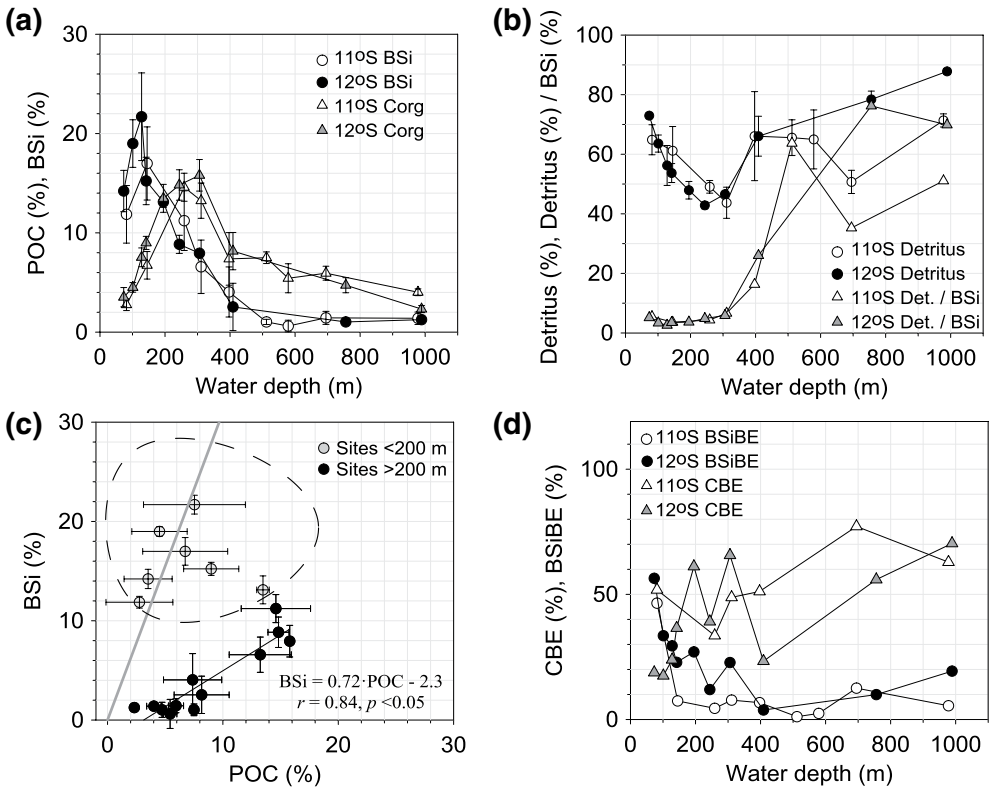

Figure 2. Particulate data across the sampling transect on the Peruvian margin. (a) POC and BSi content, where BSi refers to $\%SiO_2$, (b) detritus and detritus/BSi, (c) BSi versus POC content, and (d) CBE and BSiBE. The gray symbols in (c) within the dashed line denote shelf sites (<200 m) and the filled symbols are the sites within and below the OMZ along with the linear regression (solid line) and Pearson correlation coefficient (*r*). The gray line is the BSi:POC weight ratio of 3.1 reported by DeMaster (2002) for continental margin sediments (molar ratio ~0.6). For clarity, error bars are omitted in (d) but given in Table 2.

3.3. Biogenic Silica Distributions and Burial Efficiencies

Mean BSi content was highest on the shelf (22%) and decreased offshore to 1% below the OMZ (Table 2, Figure 2a). Downcore distributions of BSi were highly variable (Figures S9 and S10), as observed previously (Gutiérrez et al., 2009; Salvatteci et al., 2014). On average, the variability within a single core was within 40% (11°S) and 20% (12°S) of the mean value. Down core variations in the content of POM and detritus are likely responsible for the variability in BSi rather than the measurement procedure (5%–10% reproducibility) or postburial dissolution of BSi (DeMaster, 1981).

In contrast to BSi, mean POC content tended to be relatively low on the shelf (<200 m, ~2–10%) (Figure 2a). Maximum values of 16% were measured at St. 7 (300 m) at 12°S where bottom waters are permanently anoxic. Below the OMZ, POC decreased to ~5%. POC content mirrored terrigenous detritus because these two components comprised the bulk of particulates, averaging 22% and 62%, respectively (Figure 2b). BSi accounted for 9% of the bulk material on average, with carbonate comprising ~5% (not shown). The ratio of detritus to BSi was less than 10 on the shelf and in the OMZ, increasing sharply to ~60 at the deepest sites (Figure 2b). This must be partly due to the abundance of diatoms close to the coast (Franz et al., 2012). There was a marked correlation between BSi and POC in and below the OMZ, with a BSi:POC weight ratio of 0.7 (molar Si:C ratio of ~0.14, black symbols, Figure 2c). This is below the value of 3.1 reported by DeMaster (2002) for continental margins (molar Si:C ratio of 0.6), implying either preferential burial of POC (relative to BSi), preferential remineralization of BSi (relative to POC), or variations in BSi:POC export ratios (Tréguer et al., 2018). The shelf sites displayed weight ratios more similar to 3.1, and thus more typical of margins.

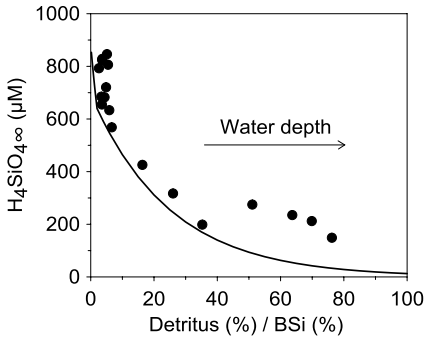

Figure 3. Mean asymptotic silicic acid concentration ($H_4SiO_{4\infty}$) at each station versus the ratio of nonbiogenic detritus to biogenic silica. The curve shows the empirical relationship by Dixit and Van Cappellen (2003) for deep-water sites (>1,000 m water depth). For the Peru data, the arrow indicates a general increase in water depth with higher ratios.

BSi accumulation was highest on the shelf, with an average across the two transects of 2,100 mmol m^{-2} yr^{-1} (Table 2). BSi recycling fluxes were 57% higher (3,300 mmol m^{-2} yr^{-1}). The mean BSi recycling flux in the OMZ was an order of magnitude higher than accumulation (1,900 vs. 130 mmol m^{-2} yr^{-1}), implying a strong decrease in BSiBE. Indeed, mean BSiBE was 34% on the shelf, declining to 7% in the OMZ and 12% below the OMZ, with an overall mean of 17% ± 8% (Figure 2d, Table 2). At the deepest station on the 12°S transect, BSiBE increased to 19%, presumably due to sediment focusing (Dale et al., 2015). CBE was 30% on the shelf, and 32% and 66% in and below the OMZ (respectively). Overall, mean CBE (39% ± 18%) was more than twice that for BSi. BSi was preserved at all stations even though $H_4SiO_{4\infty}$ were always below $H_4SiO_{4\_SAT}$ (Figure S7).

4. Discussion

4.1. Controls on BSi Burial Efficiency

4.1.1. Aluminum—Si Interactions

The data show that the mean BSiBE for the Peruvian margin is similar to the global mean of ~15% reported by Tréguer and De La Rocha (2013). Their estimate is based on direct measurements of burial and recycling fluxes in the deep-sea and by scaling BSi burial to POC burial on the margins (DeMaster, 2002). On the Peruvian margin, large differences in BSiBE with water depth are observed, decreasing from 35% on the shelf, to 7% in the OMZ and to 12% below the OMZ.

Ongoing discussion regarding silica preservation centers on the mechanisms put forward to explain why $H_4SiO_{4\infty}$ is systematically lower than $H_4SiO_{4\_SAT}$ in the presence of dissolvable silica (Figure S7 and Sarmiento & Gruber, 2006). Laboratory and field studies suggest that $H_4SiO_{4\infty}$ is controlled by chemical interactions between silica shell fragments and dissolved Al released from detrital alumino-silicate clay minerals (Dixit & Van Cappellen, 2003; Dixit et al., 2001; van Beusekom et al., 1997). To illustrate this idea, $H_4SiO_{4\infty}$ correlates negatively with the detritus/BSi ratio (Figure 3). One could expect a similar trend between $H_4SiO_{4\infty}$ and porewater Al(III) concentrations, given that the latter correlates positively with detrital content (Dixit et al., 2001). The data are in good agreement with the empirical relationship derived for deep-water sites by Dixit and Van Cappellen (2003). The elevated $H_4SiO_{4\infty}$ found at higher ratios at Peru might be due to a greater input of soluble silica (cf. Archer et al., 1993), possibly as a result of sediment focusing. The detrital content is also enriched below the OMZ due to precipitation of glauconite (Scholz et al., 2014). Overall, though, it seems that the relationship between $H_4SiO_{4\infty}$ and detritus/BSi on the Peruvian margin is similar to that in the deep-sea.

The observed decrease in $H_4SiO_{4\infty}$ is generally interpreted as kinetic and/or thermodynamic control on silicic acid levels (Sarmiento & Gruber, 2006). The kinetic viewpoint argues that Al(III) solubilized from detritus is either incorporated into the silica mineral matrix or else blocks reactive sites on frustules, leading to more sluggish BSi dissolution and lower H_4SiO_4 concentrations (McManus et al., 1995; Sayles et al., 1996; Van Cappellen & Qiu, 1997a, 1997b; Van Cappellen et al., 2002). An increase in BSi preservation would follow. Alternatively, $H_4SiO_{4\infty}$ is controlled by the precipitation of authigenic alumino-silicate minerals as the sediment porewater becomes more enriched in dissolved Al as the detritus fraction increases (Dixit et al., 2001; Michalopoulos & Aller, 2004; Rickert et al., 2002; van Beusekom et al., 1997). $H_4SiO_{4\infty}$ concentrations are then thermodynamically controlled and intermediate between the solubility of the dissolving phase (i.e., opal) and the less-soluble precipitating phase (Van Cappellen & Qiu, 1997a). In fact, silicon isotopes ($\delta^{30}Si$) in Peruvian porewaters at 11 S support this idea (Ehlert et al., 2016). Silicic acid was found to be enriched in ^{30}Si in and below the OMZ due to preferential removal of ^{28}Si into authigenic minerals, whereas weaker enrichment of ^{30}Si on the shelf with low detritus/BSi ratios indicated that precipitation was less important there. According to model results, 24% of the dissolving biogenic opal was re-precipitated

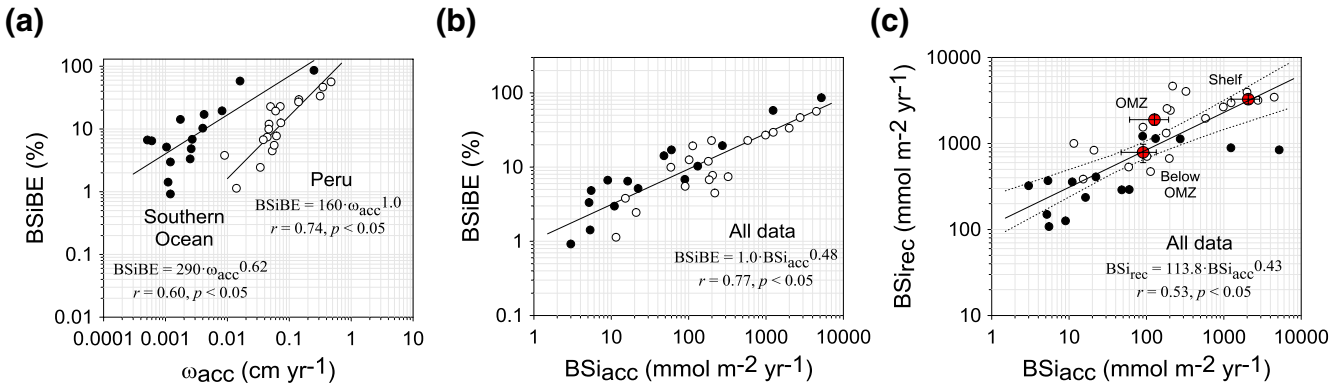

Figure 4. Log-log plots of data from individual sites on the Peruvian margin (open symbols) and the Southern Ocean (filled symbols, 170°W transect and Ross Sea, Table 1) with Pearson correlation coefficients (r) and regression curves. (a) BSiBE versus sedimentation rate, (b) BSiBE versus BSi_{acc}, and (c) BSi_{rec} versus BSi_{acc} (with 95% confidence intervals). The curve in (c) is an orthogonal regression to allow for interconversion between BSi_{rec} and BSi_{acc}. The relationships are as follows (units mmol m^{-2} yr^{-1}): $BSi_{rec} = 113.8\ BSi_{acc}^{0.43}$ and $BSi_{acc} = 1.87 \times 10^{-5}\ BSi_{rec}^{2.30}$. Note that BSi_{rec} and BSi_{acc} in (c) are independent measurements. The mean Peru data for the shelf, OMZ, and below OMZ are shown as red symbols (labeled) and not included in the regressions (error bars are from Table 2).

into authigenic phases in the OMZ. Precipitation of clay minerals would tend to increase BSiBE by lowering BSi_{rec} (Equation 6). Thus, the BSiBE for the OMZ sediments might be even lower than 7% determined here.

Despite these observations, the abundance of detritus relative to BSi cannot be the main driver for BSi preservation, because BSiBE and detritus/BSi show opposite trends with water depth (Figure 2, Table 2). Rather, the local concentrations of Al(III), H_4SiO_4 and reactive BSi are likely to be key considerations for kinetic and thermodynamic control on Si cycling. Porewater concentrations of Al(III) and H_4SiO_4 are close to ambient seawater levels at the sediment-water interface due to rapid diffusive exchange with the overlying water (cf. Figure 1). Al(III) and H_4SiO_4 concentrations tend to increase with sediment depth due to biogeochemical reactions (e.g., van Beusekom et al., 1997). Consequently, fresh BSi is more likely to be preserved if it can reach quickly the sediment layers enriched in Al(III) and H_4SiO_4. As discussed next, the sediment accumulation rate indeed appears to be a key factor for silica burial efficiency at Peru.

4.1.2. Sediment Accumulation Rate

The relationship between BSiBE and ω_{acc} at Peru can be approximated with a power law (Figure 4a). The exponent is > 0 and < 1, meaning that the rate of increase of BSiBE for a given increment in ω_{acc} is highest at low ω_{acc}. Similar observations were made by DeMaster (2003) for individual sites in the Ross Sea, which are reproduced in the figure with additional data from Southern Ocean sites along 170°W (Sayles et al., 2001; black symbols). Values of ω_{acc} at the majority of the Southern Ocean stations are 1–2 orders of magnitude lower than the Peruvian margin (Figure 4a, Table 1) due to their remoteness from major sediment sources. While BSi preservation appears to correlate with ω_{acc} in each region, it is obvious that ω_{acc} by itself cannot be used to predict BSiBE at individual sites in the deep ocean and the Peru margin (cf. Ragueneau et al., 2000; Sayles et al., 2001). The same applies to the MAR, whose global range is mainly determined by changes in ω_{acc} (Equation 2).

DeMaster (2003) pointed out that higher rates of sediment accumulation decrease the residence time of BSi at the sediment surface where porewaters are undersaturated with regard to BSi solubility. Faster sedimentation promotes preservation because BSi is more rapidly transferred to the underlying saturated porewaters where further dissolution is thermodynamically inhibited and/or where dissolved Al concentrations begin to impede BSi dissolution (Rabouille et al., 1997). This effect is apparently more pronounced in the Southern Ocean than Peru because, for a given ω_{acc}, BSiBE is higher in the Southern Ocean. The explanation for this is probably related to the fact that the BSi content is several factors higher in the Southern Ocean (up to 92%) whereas at Peru it is more diluted with detritus and POC. Lower temperatures likely also contribute to slower BSi dissolution kinetics in the Southern Ocean. The effect of ω_{acc} on BSi burial can be normalized by plotting the BSiBE against BSi_{acc}. In doing so, the data from all sites adhere more closely to a single

relationship (Figure 4b). The results imply that BSi_{acc} could be used to predict BSi preservation both in Southern Ocean deep waters and on the Eastern Tropical Pacific margin; two very different environments. To a certain extent, a robust correlation between BSiBE and BSi_{acc} is expected since the former is calculated from the latter. However, the observed correlation between BSi_{rec} and BSi_{acc}, which are based on independent measurements, supports the idea that BSi preservation is determined by the burial flux of BSi away from the undersaturated surface sediment layers (Figure 4c).

4.2. Low Burial Efficiencies Under Oxygen-Deficient Waters?

Few studies have discussed the role of bottom water oxygen levels on silica preservation even though low-oxygen upwelling areas may contribute up to 20% of BSi burial on the margins (DeMaster, 2019; Ragueneau et al., 2010). Berelson et al. (1987) determined a burial efficiency of ~10% for sediments under low-oxygen waters in the California borderland basins (Table 1). Referring to earlier work, they alluded to higher BSi recycling fluxes under low oxygen conditions. When compared to the other sites in Table 1, the borderland basins do not exhibit enhanced BSi dissolution (see Figure 5 below). Low silica preservation under oxygen-deficient waters is perhaps counterintuitive. Diminished flushing of animal burrows (bioirrigation) ought to promote preservation by maintaining BSi saturation levels within the sediment. Similarly, low oxygen would help to preserve protective organic coatings on diatom frustules, slowing down dissolution (cf. Hartnett et al., 1998; Holstein & Hensen, 2010). Yet, the depth-binned Peru data (Figure 4c, red symbols) apparently indicate that the quasipermanent anoxic OMZ sites have elevated BSi_{rec} for the derived BSi_{acc} (i.e., low silica preservation under poorly ventilated bottom waters, see also Figure 5 below). The low BSi:POC weight ratios in the OMZ are consistent with this (Figure 2c); a feature exacerbated by the relatively high CBE (Figure 2d; Dale et al., 2015).

Based on the previous idea that BSiBE is determined by the rate at which BSi is buried below the undersaturated sediment layers, the rate of BSi dissolution at the sediment surface emerges as a key factor for preservation. Studies have shown that BSi dissolution decreases rapidly over the upper few centimeters where porewaters are undersaturated (Van Cappellen & Qiu, 1997b). Dissolution can be slowed down if highly reactive, fresh silica, deposited on the sediment surface is transported to deeper, saturated layers by rapid accumulation. Sedimentation rates are an almost an order of magnitude higher on the shelf compared to the OMZ where BSiBE are correspondingly lower. Similarly, the high BSiBE in the anoxic OMZ at 650 m depth in Guaymas Basin (56%, Table 1) is consistent with the exceptional accumulation rate of 180 cm kyr^{-1} that is comparable to the Peruvian shelf.

Analogous to burial, bioturbation distributes reactive particles to deeper sediment layers where BSi dissolution is thermodynamically and/or kinetically inhibited (Ragueneau et al., 2001). Even very low rates of biodiffusive mixing can enhance the downward transport of particles (Schink et al., 1975). Sediments in the permanent OMZ at Peru lack large bioturbating organisms, whereas bioturbation on the shelf is intermittent depending on the local hydrographic conditions (Gutiérrez et al., 2009; Levin et al., 2002; Mosch et al., 2012). Mixing depths constrained by the $^{210}Pb_{xs}$ data decrease from median values of 7.6 cm on the shelf to 0.4 cm in and below the OMZ (Table S3). Higher rates of sediment accumulation and deeper surface mixing on the shelf are associated with elevated BSi preservation compared to sites in and below the OMZ with lower sediment accumulation rates and thinner mixed layers. A similar mechanism was proposed for the PAP site in Table 1 by Ragueneau et al. (2001). We conclude that differences in faunal composition and burial rates might play an important role in the fraction of BSi that is permanently buried on the Peruvian margin. This leads to spatial trends in BSi burial that differ greatly from POC that is preferentially preserved in the OMZ (Dale et al., 2015).

We consider that this interpretation is preliminary and tentative, and any potential direct role of oxygen versus sediment transport for BSi preservation is obfuscated by data uncertainties. Further mechanistic insight into the effect of O_2 levels on BSi dissolution is required to fully understand what this entails for the interpretation of BSi accumulation rates and paleoproductivity in the sediment archive.

4.3. Regional Upscaling

The Si data from 11°S and 12°S can be used to provide a benthic Si budget for the margin (<1,000 m) from 3°S to 15°S, which encompasses the main upwelling cells of the Peruvian Humboldt Current Sys-

Table 3
Si Budget for the Peruvian Margin Between 3° 20′ S and 15° 00′ S

	Shelf (0–200 m)	OMZ (200–500 m)	Below OMZ (500–1,000 m)	Σ
		3°20'S-10°00'S		
Area (km^2)	52,629	10,304	8,747	
Burial (Tmol yr^{-1})	0.109	0.001	0.001	0.11
Recycling (Tmol yr^{-1})	0.172	0.020	0.007	0.20
		10°00'S-15°00'S		
Area (km^2)	26,983	12,388	7,694	
Burial (Tmol yr^{-1})	0.056	0.002	0.001	0.06
Recycling (Tmol yr^{-1})	0.088	0.023	0.006	0.12
BSi/POC burial (molar)[a]	0.48	0.07	0.04	
BSi/POC burial (weight) [a]	2.41	0.34	0.19	

Note. Areas were calculated with Global Mapper software (see Figure S1). Fluxes refer to moles of Si.
[a]POC burial fluxes are the mean fluxes for 11°S and 12°(Dale et al., 2015).

tem (Quiñones et al., 2002). For the analysis, the upper slope is divided into the shelf (0–200 m), OMZ (200–500 m) and below the OMZ (500–1,000 m) (Figure S1). We differentiate between the latitudinal bands north and south of 10°S on the basis of regional patterns in sediment type that result from the interaction of bottom currents and shelf morphology (Velazco et al., 2015). Upscaling is achieved by multiplying the mean fluxes in Table 2 with the corresponding seafloor areas. This approach is associated with high uncertainties regarding spatial and temporal variability of, for example, sediment type, primary production, and lateral transport of biogenic particles (see Ragueneau et al., 2001; Sayles et al., 1996). Sediment accumulation rates are also only characteristic on a ~100-year-time scale (see Section 3). Nonetheless, it serves as a benchmark to compare BSi recycling and burial on the Peruvian margin with other regions.

The extrapolated fluxes show that Si cycling is dominated by the shelf due to its large area and the concentration of diatom assemblages close to the coast (Franz et al., 2012) (Table 3). The shelf accounts for 73% and 57% of the seafloor in the northern and southern sections, respectively, along with 98% of BSi accumulation and 87% of recycling. The mean BSi/POC burial weight ratio on the shelf (2.4) is somewhat lower than the ratio of 3.1 for a range of continental margin settings (DeMaster, 2002), yet drops dramatically to 0.34 in the OMZ. It indicates a weaker coupling between BSi and POC burial under oxygen-deficient waters compared to the shelf and the average continental margin.

Total BSi burial is 0.17 Tmol yr^{-1}, which is higher than determined by DeMaster (1981) for the coast of Peru and northern Chile combined (0.1 Tmol yr^{-1}). BSi burial might be lower than 0.17 Tmol yr^{-1} because the shelf broadens up to 130 km between 6°S and 10°S where the seafloor is swept clean of sediment by the poleward current (Reimers & Suess, 1983). The sand content increases to >60% at the expense of fine-grained particulates that are more prominently distributed below the shelf break (Velazco et al., 2015). If burial on the shelf north of 10°S is curtailed due to winnowing by bottom currents, total burial may be as low as 0.06 Tmol yr^{-1}. Yet, mean core-top BSi contents measured at 28 stations on the upper slope along the Peruvian and Ecuadorian coastline down to 18°by Ehlert et al. (2012) are not significantly different (5.3 ± 2.9 vs. 9.5 ± 6.4, respectively (see also DeMaster [1981]). Our best estimate for BSi burial on the Peruvian margin thus lies between 0.1 and 0.2 Tmol yr^{-1}, depending on whether the sediments in the northern section accumulate BSi.

The global BSi burial flux on continental margins has been reported to be 2.7–4.1 Tmol yr^{-1} (DeMaster, 2019). Burial of unaltered BSi on the Peruvian margin, mainly on the shelf, can thus account for up to 7% of the total burial on margins. This is a nontrivial amount if it is characteristic of oxygen-deficient upwelling regions that occupy a few percent of the total margin area (Helly & Levin, 2004). Furthermore, if the mean BSi_{acc} from the two sampling transects (760 mmol m^{-2} yr^{-1}, Table 2) is integrated over the global

margin covered by accumulating muds (24.1×10^{12} m^2; Burdige, 2007), global burial would be 18 Tmol yr^{-1}; several times higher than current estimates and clearly impossible. Taking instead the average of the sediments below 200°m (~110 mmol m^{-2} yr^{-1}), burial would be 2.7 Tmol yr^{-1} and more in line with the global average. This leads us to conclude that the Peruvian shelf is an important hotspot of silica accumulation, whereas the deeper sediments are more representative of silica accumulation on the continental margins. There may, therefore, be a need for global budgets of BSi accumulation in upwelling areas to distinguish between sediments underlying anoxic waters and adjacent shallower sediments receiving high amounts of diatomaceous detritus (DeMaster, 2019; Ragueneau et al., 2010).

4.4. Global Upscaling

The following discussion takes a global perspective of the benthic silica budget using data from Peru and the sites in Table 1. Considered collectively, the same type of relationship as observed previously is found between BSiBE and BSi_{acc} and between BSi_{rec} and BSi_{acc} (Figure 5) despite the range of applied methodologies, geochronologies, environmental parameters, and predepositional histories of BSi. It further implies that BSi preservation in the global ocean is mainly determined by a common set of master variables implicit in BSi_{acc}. Spatial variability in the thermodynamic controls on BSi solubility (e.g., temperature, pressure, pH at the seafloor, and the degree of undersaturation with respect to the reacting solid) is apparently less important in driving global patterns of silica remineralization and burial. The global trends may be rationalized in terms of our previous discussion; higher rates of accumulation imply faster burial of "fresher" BSi with a high specific surface area and more rapid dissolution kinetics (Van Cappellen et al., 2002). This allows porewaters to reach local saturation closer to the sediment surface, preventing further dissolution and enhancing burial (Rabouille et al., 1997). The apparently low preservation in the Peruvian OMZ is again prominent in this global context (Figure 5b).

The close correlation between BSi_{rec} and BSi_{acc} allows closure of the benthic Si budget with knowledge of either of these variables. From a paleoceanographic perspective, an understanding of the dependence of BSi_{RR} on BSi_{acc} is arguably more useful because BSi_{RR} can be used to back-calculate primary production (e.g., Suess, 1980). It can be described as the following power law plotted in Figure 6:

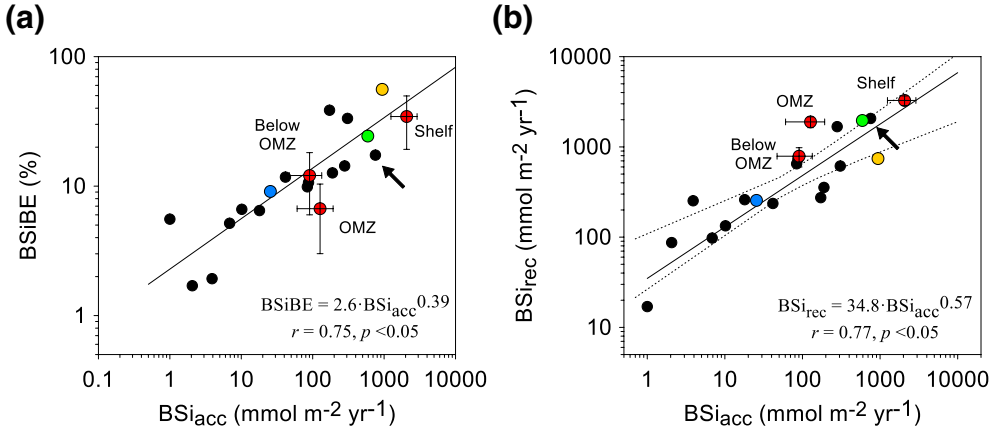

Figure 5. Log-log plots of regional mean Si data from individual sites in Table 1 and for Peru (Table 2). (a) BSiBE versus BSi_{acc}. Linear regression curve, equation, and Pearson correlation coefficient (r) are indicated. (b) BSi_{rec} versus BSi_{acc} (with 95% confidence intervals). Note that BSi_{rec} and BSi_{acc} are independent measurements with the exception of Dymond and Lyle (1994) (Table 1). The curve in (b) is an orthogonal regression to allow for interconversion between BSi_{rec} and BSi_{acc}. The relationships are as follows (units mmol m^{-2} yr^{-1}): $BSi_{rec} = 34.8\ BSi_{acc}^{0.57}$ and $BSi_{acc} = 2.0 \times 10^{-3}\ BSi_{rec}^{1.75}$. BSiBE can be calculated as $BSi_{acc}/(BSi_{acc} + BSi_{rec}) \times 100\%$. The mean Peru data for the shelf, OMZ, and below OMZ are shown as red symbols (labeled) and not included in the regressions (error bars are from Table 2). For our Peru data, only the mean data point (indicated by the arrow) is included in the regressions. Data for the Borderland basins (Berleson et al., 1987), Peru shelf (Froelich et al., 1988), and Guaymas Basin (Geilert et al., 2020) are shown as blue, green, and orange symbols, respectively.

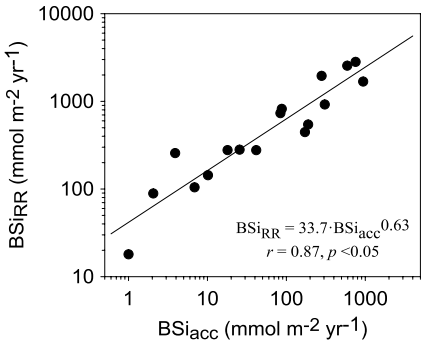

Figure 6. Log-log plot of BSi_{RR} versus BSi_{acc} for the sites in Table 1 and the average Peru data (Table 2) with the Pearson correlation coefficient (r). The curve is an orthogonal regression to allow interconversion of BSi_{RR} and BSi_{acc} (see text). BSiBE can be calculated as $BSi_{acc}/BSi_{RR} \times 100\%$.

$$BSi_{RR} = 33.7\, BSi_{acc}^{0.63} \quad (7)$$

This function builds on a similar expression derived using deep-sea data by Sayles et al. (2001). BSi_{RR} from Equation 7 are minimum estimates because it is based on BSi contents derived using standard alkaline leaching methods. It does not account for BSi protected from dissolution by Fe/Al oxide coatings or BSi that has been transformed into alumino-silicate clays by reverse weathering processes (cf. Rahman et al., 2017).

By inverting Equation 7, the fraction of BSi that is permanently buried in the sediment can be determined from the rain rate, in mmol m^{-2} yr^{-1}:

$$BSi_{acc} = 3.9 \times 10^{-3}\, BSi_{RR}^{1.58} \quad (8)$$

Using this relationship, BSiBE (= $BSi_{acc}/BSi_{RR} \times 100$) increases in a nonlinear fashion, from 6% to 21% for rain rates of 100 and 1,000 mmol m^{-2} yr^{-1}, respectively. A similar nonlinear dependence of BSiBE on BSi_{RR} has been derived for the equatorial Pacific using independent sediment trap data (Dymond & Lyle, 1994; see also; Broecker & Peng, 1982).

BSi_{RR} estimates for the deep-sea are uncertain, ranging from 23 to 79 Tmol yr^{-1} (DeMaster, 2019; Laruelle et al., 2009; Sarmiento & Gruber, 2006; Tréguer and De La Rocha, 2013). Taking the average of these values (51 Tmol yr^{-1}), a mean BSi_{acc} for deep-sea sediments (area > 1,000 m = 319×10^{12} m^2, Menard & Smith, 1966) can be calculated with Equation 8 with an uncertainty obtained by bootstrapping the data (n = 1,000). This gives 3.6 ± 1.3 Tmol yr^{-1}, which is equivalent to the most recent deep-sea BSi burial estimates (DeMaster, 2019). The deep-sea burial efficiency is 7% ± 4% and close to those from the deep-sea sites in Table 1 located away from river mouths.

BSi_{acc} on continental margins is 2.7–4.1 Tmol yr^{-1} (see Section 1), and the area of fine-grained accumulating margin sediments is 24.1×10^{12} m^2 (Burdige, 2007). According to the relationships above, these burial rates are associated with a BSi_{RR} of 16–21 Tmol yr^{-1}, which translates into minimum and maximum BSiBE of 13% and 25%, respectively. This is similar to the shelf estimate of 22% by Laruelle et al. (2009). These simple calculations, albeit associated with fairly large uncertainties, suggest that the relationships in Equations 7 and 8 are consistent with the published global Si budget. Perhaps a more accurate estimate of benthic-pelagic coupling of Si at the global scale could be achieved by combining Equation 8 with Earth system models or spatial distributions of BSi_{RR} (Gao et al., 2016; Nelson et al., 1995). Ground-truthing of such exercises will benefit from further insights gained from Si isotope distributions in sediment porewaters and fluxes from different margin settings (Ehlert et al., 2016; Rahman et al., 2017).

5. Conclusions

An extensive set of data on silica cycling in sediments on the Peruvian margin has been analyzed. It is one of the most comprehensive compilations of Si fluxes for a continental margin setting and the first for an open margin OMZ. BSi is extensively solubilized, resulting in burial efficiencies that decrease from around 35% on the shelf to 12% at 1,000 m water depth. Overall, the results suggest that Peruvian sediments make a nontrivial contribution to silica cycling on the global margin. The data presented are consistent with other sites in terms of the factors leading to BSi preservation. Our analysis suggests that a key control on silica preservation at Peru is the rate at which highly soluble BSi is transported away from the surface sediment to the underlying saturated sediment layers where dissolution of BSi is thermodynamically and/or kinetically inhibited. A lack of bioturbation could be responsible for low burial efficiencies in sediments underneath permanently anoxic bottom waters. Compared to BSi, organic carbon burial efficiency is high in the OMZ, and this divergence may have important implications for the analysis of long-term sediment cores from OMZs and the reconstruction of paleoproductivity. Analysis of existing global data, together with the Peruvian data, leads to a simple relationship between silica accumulation and rain rate that can be used for es-

timating (i) rain rate and thus paleoproductivity from sediment archives, and (ii) silica recycling and burial fluxes in global models of the marine Si cycle.

Data Availability Statement

The Si data presented in this study is archived at the PANGAEA World Data Center (https://www.pangaea.de/?q%3DM77%2F1, https://www.pangaea.de/?q%3DM77%2F2, https://www.pangaea.de/?q=M92, https://www.pangaea.de/?q=M136, https://www.pangaea.de/?q=M137).

Conflict of Interest

The authors declare no conflicts of interest relevant to this study.

Acknowledgments
We thank the captains and crew of RV Meteor cruises M77 (legs 1 and 2), M92, M136, and M137 for their assistance during fieldwork. This work is a contribution of the Sonderforschungsbereich 754 "*Climate – Biogeochemistry Interactions in the Tropical Ocean*" (www.sfb754.de) which is supported by the Deutsche Forschungsgemeinschaft. We thank our colleagues deeply for their assistance on board over the 12 years of the SFB754 project (2008–2019) and for contributing to a lively and convivial atmosphere on board. We thank the journal editor (Sara Mikaloff Fletcher) for handling this manuscript. We are very grateful to Dave DeMaster and an anonymous reviewer for excellent constructive feedback.

References

Alperin, M. J., Suayah, I. B., Benninger, L. K., & Martens, C. S. (2002). Modern organic carbon burial fluxes, recent sedimentation rates, and particle mixing rates from the upper continental slope near Cape Hatteras, North Carolina (USA). *Deep Sea Research Part II: Topical Studies in Oceanography*, *49*, 4645–4665.

Archer, D., Lyle, M., Rodgers, K., & Froelich, P. (1993). What controls opal preservation in tropical deep-sea sediments? *Paleoceanography*, *8*, 7–21.

Arthur, M. A., Dean, W. E., & Laarkamp, K. (1998). Organic carbon accumulation and preservation in surface sediments on the Peru margin. *Chemical Geology*, *152*, 273–286.

Berelson, W. M. (1991). The flushing of two deep-sea basins, southern California borderland. *Limnology and Oceanography*, *36*, 1150–1166.

Berelson, W. M., Anderson, R. F., Dymond, J., DeMaster, D. J., Hammond, D. E., Collier, R., et al. (1997). Biogenic budgets of particle rain, benthic remineralization and sediment accumulation in the Equatorial Pacific. *Deep Sea Research Part II: Topical Studies in Oceanography*, *44*, 2251–2280.

Berelson, W. M., Hammond, D. E., & Johnson, K. S. (1987). Benthic fluxes and the cycling of biogenic silica and carbon in two southern California borderland basins. *Geochimica et Cosmochimica Acta*, *51*, 1345–1363.

Bohlen, L., Dale, A. W., Sommer, S., Mosch, T., Hensen, C., Noffke, A., et al. (2011). Benthic nitrogen cycling traversing the Peruvian oxygen minimum zone. *Geochimica et Cosmochimica Acta*, *75*, 6094–6111.

Broecker, W. S., & Peng, T.-S. (1982). *Tracers in the sea. Lamont-Doherty geological observatory*. Columbia University.

Burdige, D. J. (2007). Preservation of organic matter in marine sediments: Controls, mechanisms, and an imbalance in sediment organic carbon budgets? *Chemical Reviews*, *107*, 467–485.

Burwicz, E. B., Rüpke, L., & Wallmann, K. (2011). Estimation of the global amount of submarine gas hydrates formed via microbial methane formation based on numerical reaction-transport modeling and a novel parameterization of Holocene sedimentation. *Geochimica et Cosmochimica Acta*, *75*, 4562–4576.

Canfield, D. E. (1993). Organic matter oxidation in marine sediments. In R. Wollast, F. T. Mackenzie & L. Chou (Eds.), *Interactions of C, N, P and S biogeochemical Cycles and Global Change* (pp. 333–363). Berlin, Heidelberg: Springer-Verlag.

Chase, Z., Kohfeld, K. E., & Matsumoto, K. (2015). Controls on biogenic silica burial in the Southern Ocean. *Global Biogeochemical Cycles*, *29*, 1599–1616.

Dale, A. W., Bourbonnais, A., Altabet, M., Wallmann, K., & Sommer, S. (2019). Isotopic fingerprints of benthic nitrogen cycling in the Peruvian oxygen minimum zone. *Geochimica et Cosmochimica Acta*, *245*, 406–425.

Dale, A. W., Sommer, S., Lomnitz, U., Bourbonnais, A., & Wallmann, K. (2016). Biological nitrate transport in sediments on the Peruvian margin mitigates benthic sulfide emissions and drives pelagic N loss during stagnation events. *Deep Sea Research Part I: Oceanographic Research Papers*, *112*, 123–136.

Dale, A. W., Sommer, S., Lomnitz, U., Montes, I., Treude, T., Liebetrau, V., et al. (2015). Organic carbon production, mineralisation and preservation on the Peruvian margin. *Biogeosciences*, *12*, 1537–1559.

DeMaster, D. J. (1981). The supply and accumulation of silica in the marine environment. *Geochimica et Cosmochimica Acta*, *5*, 1715–1732.

DeMaster, D. J. (2002). The accumulation and cycling of biogenic silica in the Southern Ocean: Revisiting the marine silica budget. *Deep Sea Research Part II: Topical Studies in Oceanography*, *49*, 3155–3167.

DeMaster, D. J. (2003). The diagenesis of biogenic silica: Chemical transformations occurring in the water column, seabed, and crust. In H. D. Holland, & K. K. Turekian (Eds.), *Treatise on geochemistry* (pp. 87–98). Elsevier. ISBN 0-08-043751-6.

DeMaster, D. J. (2019). The global marine silica budget: Sources and sinks. In K. Cochran, H. Bokuniewicz, & P. Yager (Eds.), *Encyclopedia of ocean sciences*. 3rd ed. (pp. 473–483). Elsevier Academic Press.

DeMaster, D. J., Ragueneau, O., & Nittrouer, C. A. (1996). Preservation efficiencies and accumulation rates for biogenic silica and organic C, N, and P in high-latitude sediments: The Ross Sea. *Journal of Geophysical Research*, *101*, 18501–18518.

Dixit, S., & Cappellen, P. V. (2003). Predicting benthic fluxes of silicic acid from deep-sea sediments. *Journal of Geophysical Research*, *108*, 3334. https://doi.org/10.1029/2002JC001309

Dixit, S., Cappellen, P. V., & van Bennekom, A. J. (2001). Processes controlling solubility of biogenic silica and pore water build-up of silicic acid in marine sediments. *Marine Chemistry*, *73*, 333–352.

Dugdale, R. C., Wilkerson, F. P., & Minas, H. J. (1995). The role of a silicate pump in driving new production. *Deep Sea Research Part I: Oceanographic Research Papers*, *42*, 697–719. http://dx.doi.org/10.1016/0967-0637(95)00015-X

Dymond, J., & Lyle, M. (1994). *Particle fluxes in the ocean and implications for sources and preservation of ocean sediments. Material fluxes on the surface of the Earth*. Washington, DC: National Academy Press.

Echevin, V., Aumont, O., Ledesma, J., & Flores, G. (2008). The seasonal cycle of surface chlorophyll in the Peruvian upwelling system: A modelling study. *Progress in Oceanography*, *79*, 167–176.
Ehlert, C., Doering, K., Wallmann, K., Scholz, F., Sommer, S., Grasse, P., et al. (2016). Stable silicon isotope signatures of marine pore waters – Biogenic opal dissolution versus authigenic clay mineral formation. *Geochimica et Cosmochimica Acta*, *191*, 102–117.
Ehlert, C., Grasse, P., Mollier-Vogel, E., Böschen, T., Franz, J., de Souza, G. F., et al. (2012). Factors controlling the silicon isotope distribution in waters and surface sediments of the Peruvian coastal upwelling. *Geochimica et Cosmochimica Acta*, *99*, 128–145.
Erdem, Z., Schönfeld, J., Glock, N., Dengler, M., Mosch, T., Sommer, S., et al. (2016). Peruvian sediments as recorders of an evolving hiatus for the last 22 thousand years. *Quaternary Science Reviews*, *137*, 1–14.
Estrada, M., & Blasco, D. (1985). Phytoplankton assemblages in coastal upwelling areas. In C. Bas, R. Margalef, & P. Rubies (Eds.), *Simposio Internacional Sobre Las Areas de Afloramiento Mas Importantes del Oeste Africano (Cabo Blanco y Benguela)*. (pp. 379–402). Barcelona, Spain: Instituto de Investigaciones Pesqueras.
Francois, R., Altabet, M. A., Yu, E. F., Sigman, D., Bacon, M. P., Frank, M., et al. (1997). Dominance of upper water column stratification in the Southern Ocean's contribution to low glacial atmospheric CO_2. *Nature*, *389*, 929–935.
Franz, J., Krahmann, G., Lavik, G., Grasse, P., Dittmar, T., & Riebesell, U. (2012). Dynamics and stoichiometry of nutrients and phytoplankton in waters influenced by the oxygen minimum zone in the eastern tropical Pacific. *Deep Sea Research Part I: Oceanographic Research Papers*, *62*, 20–31.
Froelich, P., Arthur, M., Burnett, W., Deakin, M., Hensley, V., Jahnke, R., et al. (1988). Early diagenesis of organic matter in Peru continental margin sediments: Phosphorite precipitation. *Marine Geology*, *80*, 309–343.
Fuenzalida, R., Schneider, W., Garcés-Vargas, J., Bravo, L., & Lange, C. B. (2009). Vertical and horizontal extension of the oxygen minimum zone in the eastern South Pacific Ocean. *Deep Sea Research Part II Topical Studies in Oceanography*, *56*, 1027–1038.
Gao, S., Wolf-Gladrow, D. A., & Völker, C. (2016). Simulating the modern δ^{30}Si distribution in the oceans and in marine sediments. *Global Biogeochemical Cycles*, *30*, 120–133. https://doi.org/10.1002/2015GB005189
Geilert, S., Grasse, P., Doering, K., Wallmann, K., Ehlert, C., Scholz, F., et al. (2020). Impact of ambient conditions on the Si isotope fractionation in marine pore fluids during early diagenesis. *Biogeosciences*, *17*, 1745–1763.
Glud, R., Gundersen, J., Jørgensen, B. B., Revsbech, N. P., & Schulz, H. D. (1994). Diffusive and total oxygen uptake of deep-sea sediments in the eastern South Atlantic ocean: in situ laboratory measurements. *Deep Sea Research Part I: Oceanographic Research Papers*, *41*, 1767–1788.
Grasshoff, K., Ehrhardt, M., & Kremling, K. (1999). *Methods of seawater analysis*. Weinheim, Germany: Wiley-VCH.
Gutiérrez, D., Enríquez, E., Purca, S., Quipúzcoa, L., Marquina, R., Flores, G., & Graco, M. (2008). Oxygenation episodes on the continental shelf of central Peru: Remote forcing and benthic ecosystem response. *Progress in Oceanography*, *79*, 177–189.
Gutiérrez, D., Sifeddine, A., Field, D. B., Ortlieb, L., Vargas, G., Chávez, F. P., et al. (2009). Rapid reorganization in ocean biogeochemistry off Peru towards the end of the Little Ice Age. *Biogeosciences*, *6*, 835–848.
Hammond, D. E., Cummins, K. M., McManus, J., Berelson, W. M., & Smith, G. (2004). Methods for measuring benthic nutrient flux on the California Margin: Comparing shipboard core incubations to in situ lander results. *Limnology and Oceanography: Methods*, *2*, 146–159.
Hartnett, H. E., Keil, R. G., Hedges, J. I., & Devol, A. H. (1998). Influence of oxygen exposure time on organic carbon preservation in continental margin sediments. *Nature*, *391*, 572–574.
Heinze, C., Hupe, A., Maier-Reimer, E., Dittert, N., & Ragueneau, O. (2003). Sensitivity of the marine biospheric Si cycle for biogeochemical parameter variations. *Global Biogeochemical Cycles*, *17*, 12–21.
Helly, J. J., & Levin, L. A. (2004). Global distribution of naturally occurring marine hypoxia on continental margins. *Deep Sea Research Part I: Oceanographic Research Papers*, *51*, 1159–1168.
Holstein, J. M., & Hensen, C. (2010). Microbial mediation of benthic biogenic silica dissolution. *Geo-Marine Letters*, *30*, 477–492.
Hou, Y., Hammond, D. E., Berelson, W. M., Kemnitz, N., Adkins, J. F., & Lunstrum, A. (2019). Spatial patterns of benthic silica flux in the North Pacific reflect upper ocean production. *Deep Sea Research Part I: Oceanographic Research Papers*, *148*, 25–33.
Hurd, D. C. (1973). Interactions of biogenic opal, sediment and seawater in the Central Equatorial Pacific. *Geochimica et Cosmochimica Acta*, *37*, 2257–2282.
Jahnke, R. A., Reimers, C. E., & Craven, D. B. (1990). Intensification of recycling of organic matter at the sea floor near ocean margins. *Nature*, *348*, 50–54.
Laruelle, G. G., Roubeix, V., Sferratore, A., Brodherr, B., Ciuffa, D., Conley, D. J., et al. (2009). Anthropogenic perturbations of the silicon cycle at the global scale: Key role of the land-ocean transition. *Global Biogeochemical Cycles*, *23*, 1–17.
Leslie, B. W., Hammond, D. E., Berelson, W. M., & Lund, S. P. (1990). Diagenesis in anoxic sediments from the California continental borderland and its influence on iron, sulfur, and magnetite behavior. *Journal of Geophysical Research*, *95*, 4453–4470.
Levin, L., Gutiérrez, D., Rathburn, A., Neira, C., Sellanes, J., Munoz, P., et al. (2002). Benthic processes on the Peru margin: A transect across the oxygen minimum zone during the 1997-98 El Niño. *Progress in Oceanography*, *53*, 1–27.
Lomnitz, U., Sommer, S., Dale, A. W., Löscher, C. R., Noffke, A., Wallmann, K., & Hensen, C. (2016). Benthic phosphorus cycling in the Peruvian oxygen minimum zone. *Biogeosciences*, *13*, 1367–1386.
McManus, J., Hammond, D. E., William, M., Kilgore, T. E., DeMaster, D. J., Ragueneau, O. G., & Collier, R. W. (1995). Early diagenesis of biogenic opal: Dissolution rates, kinetics, and paleoceanographic implications. *Deep Sea Research Part II Topical Studies in Oceanography*, *42*, 871–903.
Menard, H. W., & Smith, S. M. (1966). Hypsometry of ocean basin provinces. *Journal of Geophysical Research*, *71*, 4305–4325.
Michalopoulos, P., & Aller, R. (2004). Early diagenesis of biogenic silica in the Amazon delta: Alteration, authigenic clay formation, and storage. *Geochimica et Cosmochimica Acta*, *68*, 1061–1085.
Mosch, T., Sommer, S., Dengler, M., Noffke, A., Bohlen, L., Pfannkuche, O., et al. (2012). Factors influencing the distribution of epibenthic megafauna across the Peruvian oxygen minimum zone. *Deep Sea Research Part I: Oceanographic Research Papers*, *68*, 123–135.
Müller, P. J., & Schneider, R. (1993). An automated leaching method for the determination of opal in sediments and particulate matter. *Deep-Sea Research*, *40*(3), 425–444.
Nelson, D. M., Tréguer, P., Brzezinski, M. A., Leynaert, A., & Quéguiner, B. (1995). Production and dissolution of biogenic silica in the ocean: Revised global estimates, comparison with regional data and relationship to biogenic sedimentation Revised Global Estimates of Biogenic Silica Production and Export. *Global Biogeochemical Cycles*, *9*, 359–372.
Pondaven, P., Ragueneau, O., Tréguer, P., Hauvespre, A., Dezileau, L., & Reyss, J. L. (2000). Resolving the "opal paradox" in the Southern Ocean. *Nature*, *405*, 168–172.

Quiñones, R. A., Gutierrez, M. H., Daneri, G., Aguilar, D. G., Gonzalez, H. E., & Chavez, F. P. (2010). The Humboldt current system. In K.-K. Liu, L. Atkinson, R. Quiñones, & L. Talaue-McManus (Eds.), *Carbon and nutrient fluxes in continental margins: A global synthesis* (pp. 44–64). Berlin, Germany: Springer-Verlag.

Rabouille, C., Gaillard, J.-F., Tre´guer, P., & Vincendeau, M.-A. (1997). Biogenic silica recycling in surficial sediments across the Polar Front of the Southern Ocean Indian sector. *Deep Sea Research Part II Topical Studies in Oceanography*, *44*, 1151–1176.

Ragueneau, O., Conley, D. J., DeMaster, D. J., Dürr, H. H., & Dittert, N. (2010). Biogeochemical transformations of silicon along the land-ocean continuum and implications for the global carbon cycle. In K. K. Liu, L. Atkinson, R. Quiñones, & L. Talaue-McManus (Eds.), *Carbon and nutrient fluxes in continental margins. Global change – The IGBP series* (pp. 515–527). Berlin, Heidelberg: Springer.

Ragueneau, O., Dittert, N., Pondaven, P., Treguer, P., & Corrin, L. (2002). Si/C decoupling in the world ocean: Is the Southern Ocean different? *Deep Sea Research Part II Topical Studies in Oceanography*, *49*, 3127–3154.

Ragueneau, O., Gallinari, M., Corrin, L., Grandel, S., Hall, P., Hauvespre, A., et al. (2001). The benthic silica cycle in the Northeast Atlantic: Annual mass balance, seasonality, and importance of non-steady-state processes for the early diagenesis of biogenic opal in deep-sea sediments. *Progress in Oceanography*, *50*, 171–200.

Ragueneau, O., Regaudie-de-Gioux, A., Moriceau, B., Gallinari, M., Vangriesheim, A., Baurand, F., & Khripounoff, A. (2009). A benthic Si mass balance on the Congo margin: Origin of the 4000 m DSi anomaly and implications for the transfer of Si from land to ocean. *Deep Sea Research Part II Topical Studies in Oceanography*, *56*, 2197–2207.

Ragueneau, O., Treguer, P., Leynaert, A., Anderson, R. F., Brzezinski, M. A., DeMaster, D. J., et al. (2000). A review of the Si cycle in the modern ocean: Recent progress and missing gaps in the application of biogenic opal as a paleoproductivity proxy. *Global and Planetary Change*, *26*, 317–365.

Rahman, S., Aller, R. C., & Cochran, J. K. (2017). The missing silica sink: Revisiting the marine sedimentary Si cycle using cosmogenic ^{32}Si. *Global Biogeochemical Cycles*, *31*, 1559–1578.

Reimers, C. E., & Suess, E. (1983). Spatial and temporal patterns of organic matter accumulation on the Peru continental margin. In E. Suess, & J. Thiede (Eds.), *Coastal upwelling, its sediment Record. Part B* (pp. 311–345). New York, NY: Plenum Press.

Rickert, D., Schlüter, M., & Wallmann, K. (2002). Dissolution kinetics of biogenic silica from the water column to the sediments. *Geochimica et Cosmochimica Acta*, *66*, 439–455.

Salvatteci, R., Field, D., Sifeddine, A., Ortlieb, L., Ferreira, V., Baumgartner, T., et al. (2014). Cross-stratigraphies from a seismically active mud lens off Peru indicate horizontal extensions of laminae, missing sequences, and a need for multiple cores for high resolution records. *Marine Geology*, *357*, 72–89.

Sarmiento, J. L., & Gruber, N. (2006). *Ocean biogeochemical dynamics*. Princeton University Press.

Sayles, F. L., Deuser, W. G., Goudreau, J. E., Dickinson, W. H., Jickells, T. D., & King, P. (1996). The benthic cycle of biogenic opal at the Bermuda Atlantic Time Series site. *Deep Sea Research Part I: Oceanographic Research Papers*, *43*, 383–409.

Sayles, F. L., Martin, W. R., Chase, Z., & Anderson, R. F. (2001). Benthic remineralization and burial of biogenic SiO_2, $CaCO_3$, organic carbon, and detrital material in the Southern Ocean along a transect at 170ºW West. *Deep Sea Research Part II Topical Studies in Oceanography*, *48*, 4323–4383.

Schink, D. R., Guinasso, N. L., Jr, & Fanning, K. A. (1975). Processes affecting the concentration of silica at the sediment-water interface of the Atlantic Ocean. *Journal of Geophysical Research*, *80*, 3013–3031.

Scholz, F., Hensen, C., Noffke, A., Rohde, A., Liebetrau, V., & Wallmann, K. (2011). Early diagenesis of redox-sensitive trace metals in the Peru upwelling area – Response to ENSO-related oxygen fluctuations in the water column. *Geochimica et Cosmochimica Acta*, *75*, 7257–7276.

Scholz, F., Severmann, S., McManus, J., Noffke, A., Lomnitz, U., & Hensen, C. (2014). On the isotope composition of reactive iron in marine sediments: Redox shuttle versus early diagenesis. *Chemical Geology*, *389*, 48–59.

Shibamoto, Y., & Harada, K. (2010). Silicon flux and distribution of biogenic silica in deep-sea sediments in the western North Pacific Ocean. *Deep Sea Research Part I: Oceanographic Research Papers*, *57*, 163–174.

Sommer, S., Gier, J., Treude, T., Lomnitz, U., Dengler, M., Cardich, J., & Dale, A. W. (2016). Depletion of oxygen, nitrate and nitrite in the Peruvian oxygen minimum zone cause an imbalance of benthic nitrogen fluxes. *Deep Sea Research Part I: Oceanographic Research Papers*, *112*, 113–122.

Suess, E. (1980). Particulate organic carbon flux in the oceans – Surface productivity and oxygen utilization. *Nature*, *288*, 260–263.

Tengberg, A., Hall, P. O. J., Andersson, U., Lindén, B., Styrenius, O., Boland, G., et al. (2005). Intercalibration of benthic flux chambers: II. Hydrodynamic characterization and flux comparisons of 14 different designs. *Marine Chemistry*, *94*, 147–173.

Thamdrup, B., Dalsgaard, T., & Revsbech, N. P. (2012). Widespread functional anoxia in the oxygen minimum zone of the Eastern South Pacific. *Deep Sea Research Part I: Oceanographic Research Papers*, *65*, 36–45.

Tréguer, P., Bowler, C., Moriceau, B., Dutkiewicz, S., Gehlen, M., Aumont, O., et al. (2018). Influence of diatom diversity on the ocean biological carbon pump. *Nature Geoscience*, *11*, 27–37.

Tréguer, P., De La Rocha, & Christina, L. (2013). The world ocean silica cycle. *Annual Review of Marine Science*, *5*, 477–501.

Treguer, P., Nelson, D. M., Van Bennekom, A. J., DeMaster, D. J., Leynaert, A., & Queguiner, B. (1995). The silica balance in the world ocean: A reestimate. *Science*, *268*, 375–379.

van Beusekom, J. E. E., van Bennekom, A. J., Tréguer, P., & Morvan, J. (1997). Aluminium and silicic acid in water and sediments of the Enderby and Crozet Basins. *Deep Sea Research Part II Topical Studies in Oceanography*, *44*, 987–1003.

Van Cappellen, P., Dixit, S., & van Beusekom, J. (2002). Biogenic silica dissolution in the oceans: Reconciling experimental and field-based dissolution rates. *Global Biogeochemical Cycles*, *16*, 1075. https://doi.org/10.1029/2001GB001431

Van Cappellen, P., & Qiu, L. (1997a). Biogenic silica dissolution in sediments of the Southern Ocean. I. Solubility. *Deep Sea Research Part II Topical Studies in Oceanography*, *44*, 1109–1128.

Van Cappellen, P., & Qiu, L. (1997b). Biogenic silica dissolution in sediments of the Southern Ocean. II. Kinetics. *Deep Sea Research Part II Topical Studies in Oceanography*, *44*, 1109–1128.

Velazco, F., Solís, J., Delgado, C., & Gomero, R. (2015). Surface sediments and morphology of the Peruvian continental shelf and upper slope between 3°S0′S to 15°30′S. *Insituto del Mar del Peru Inf*, *42*(4), 526–537.

Reference From the Supporting Information

Boudreau, B. P. (1997). *Diagenetic models and their implementation*. Berlin, Germany: Springer-Verlag.